Published in final edited form as:
J Magn Reson. 2014 September ; 246: 62–68. doi:10.1016/j.jmr.2014.06.019.

An eight-channel T/R head coil for parallel transmit MRI at 3T using ultra-low output impedance amplifiers

Katherine Lynn Moody[1], **Neal A. Hollingsworth**[2], **Feng Zhao**[3], **Jon-Fredrik Nielsen**[3], **Douglas C. Noll**[3], **Steven M. Wright**[2,1,4], and **Mary Preston McDougall**[1,2]

[1]Department of Biomedical Engineering, Texas A&M University, College Station, Texas, USA

[2]Department of Electrical and Computer Engineering, Texas A&M University, College Station, Texas, USA

[3]Department of Biomedical Engineering, University of Michigan, Ann Arbor, Michigan, USA

[4]Department of Radiology, Texas A&M Health Science Center, College Station, Texas, USA

Abstract

Parallel transmit is an emerging technology to address the technical challenges associated with MR imaging at high field strengths. When developing arrays for parallel transmit systems, one of the primary factors to be considered is the mechanism to manage coupling and create independently operating channels. Recent work has demonstrated the use of amplifiers to provide some or all of the channel-to-channel isolation, reducing the need for on-coil decoupling networks in a manner analogous to the use of isolation preamplifiers with receive coils. This paper discusses an eight-channel transmit/receive head array for use with an ultra-low output impedance (ULOI) parallel transmit system. The ULOI amplifiers eliminated the need for a complex lumped element network to decouple the eight rung array. The design and construction details of the array are discussed in addition to the measurement considerations required for appropriately characterizing an array when using ULOI amplifiers. B_1 maps and coupling matrices are used to verify the performance of the system.

Keywords

Parallel transmit; array coils; RF coils; ultra-low output impedance amplifiers; amplifier decoupling; coupling measurements; isolation measurements

Address correspondence to: Mary Preston McDougall, Department of Biomedical Engineering, 5045 Emerging Technologies Building, 3120 TAMU, College Station, TX 77843-3120 USA, Ph 979-458-1146, Fax 979-845-4450, mpmcdougall@tamu.edu.

INTRODUCTION

The increase in signal-to-noise ratio (SNR) and spectral resolution that comes with high field magnetic resonance imaging (MRI) can be traded for improvements in spatial and temporal resolution [2]. In many cases, technical challenges prevent these benefits from being straightforwardly realized in practice. One significant and well-known challenge is potential inhomogeneity in the transmit B_1 field due to the higher frequencies (and shorter radiofrequency (RF) wavelengths) associated with higher magnetic field strengths [3–7]. In neuroimaging applications, this often manifests as a central brightening artifact due to constructive interference in the center of the head preventing uniform tip angles [8–9].

A number of research groups have used multiple transmit channels to address this challenge. Approaches range from relatively straightforward B_1 shimming [10–13] to more complex transmit SENSE techniques in which separate RF excitation pulses are sent to each channel [14–16]. With either approach, however, the level of independence between transmit channels is a concern. Any current applied to one element will induce a voltage (more accurately, an electromotive force or EMF) in any other elements if they have any mutual impedance. In turn, this induced voltage can drive unwanted currents in the other coils, contaminating the desired coil pattern. This is commonly referred to as “coupling” between coils. One can preserve the patterns either by reducing the induced voltage by eliminating or cancelling the mutual impedance, or, by ensuring that no additional currents are generated as a result of the induced voltage. There are a number of possible ways to eliminate the mutual impedance, such as geometrically overlapping the coils or constructing a lumped element network on the coil to cancel the mutual inductance [17]. To eliminate the currents driven by the mutual impedance, one can introduce a high impedance across the terminals of the coils as in the case of using isolating preamplifiers [18]. A benefit of the latter approach is that it results in less concern for the mutual impedance between coils, just as with receive arrays. To generalize, array coil design, specifically with respect to the degree of on-coil decoupling required, depends on and operates in concert with the preamplifier regime in the receive case and the amplifier regime in the transmit case [15].

Most transmit array coils are designed for use with standard RF power amplifiers, which have been designed to produce maximum output power assuming a 50Ω load. To maintain expected performance, these ‘conventional’ amplifiers generally rely on decoupling of the coil elements themselves, just as with receive arrays operating with conventional preamplifiers, to ensure that the amplifier sees the expected load. Some combination of geometric overlap and lumped element decoupling networks must be employed on these arrays to enable independent operation of the channels. Geometric overlap is limited in application to adjacent elements and imposes constraints on the array geometry. Lumped element networks require no overlap, but as the channel counts increase, the network required to fully decouple all elements increases in complexity due to the increasing number of decoupling capacitors required [17]. As an example, to decouple seven elements with a lumped element ladder network, three decoupling capacitors are required for each ladder stage [19], giving a total of 21 capacitors needed for full decoupling. In extending the approach to eight elements, four decoupling capacitors are required at each ladder stage for a total of 32 decoupling capacitors. The values for the decoupling capacitors are guided by

closed-form equations that require iterative non-linear and numerical field solvers to compute [20], and further fine adjustments in element tuning are done iteratively and experimentally. The amount of available decoupling is also sensitive to loading. As indicated in one study [19], the decoupling between opposing elements of a four-element array was found to increase from -30 dB in the unloaded case to -10 dB in the loaded case, indicating 10% of the power from one element being coupled into its opposing element. Due to these complications involved with the various on-coil decoupling strategies, stripline elements and shielded loop elements have emerged as the two most common designs for parallel transmit arrays in neuroimaging due to their inherent favorable coupling properties [11, 21–25]. Even still, an additional decoupling network is typically needed, adding complexity to the array design [11]. Recently, alternative approaches to amplifier design have been investigated that provide some degree of isolation between channels, decreasing or even eliminating the need for decoupling between the coil elements themselves.

One approach under investigation is current source amplification in which each series resonant element is driven with a prescribed current, insensitive to the effects of loading, including element-to-element coupling [21–25]. This allows for large amounts of flexibility in the design of the array coils used with current sources, as in principle no on-coil decoupling techniques are needed. Current source amplifiers provide high isolation by presenting a high impedance to the series tuned coil, but are not matched for optimal power output, so they are limited in the amount of current they can produce as compared to standard RF power amplifiers [26]. Recent work on current mode class-D (CMCD) amplifiers has shown to improve efficiency and may be able to produce higher peak output levels than linear current source amplifiers [24–25, 27]; however, the CMCD design has other complications that must be addressed in the process [25].

Chu et al. introduced the “ultra-low output impedance (ULOI) amplifier”, which, in contrast to the current source amplifier, provides decoupling in a manner analogous to preamplifier decoupling in parallel receive applications [28]. The array elements are matched to 50Ω input impedance using a network that forms a trap when connected to the ULOI amplifier or preamplifier. ULOI amplifiers are power matched and present a low impedance to the coil port. The power match enables peak output levels comparable to standard power amplifiers while the low impedance provides isolation when combined with an appropriately designed matching network on the coil. The isolation obtained with ULOI amplifiers is substantially lower than that of current source amplifiers, but the peak current delivered to the coil is higher. In addition, as discussed in [28], the ULOI amplifier drain is biased into saturation so that output current and parametric variation is minimized in cases of non-passive loading such as the case with coupled transmit array elements. In practice, the ULOI amplifiers represent a “middle ground” between current source and standard power amplifiers with respect to isolation and output power. We chose to implement a parallel transmit system with ultra-low output impedance amplifiers to achieve greater power output over previously built current sources [23] and to achieve decoupling benefits to simplify the on-coil decoupling network. An added benefit of this approach is that it allows for a straightforward transmit/receive configuration in that the matching network required for the ULOI amplifier is identical to the one needed for low-input impedance preamplifiers. This paper discusses the construction and characterization of an eight-channel transmit/receive head array for use

with an ultra-low output impedance parallel transmit system. The eight-element array was decoupled using a simple decoupling network in combination with the isolation provided by the ULOI amplifiers. The characterization of the isolation provided by the stages of the system, from amplifier to coil, is discussed in detail.

MATERIALS AND METHODS

System Overview

The eight-channel parallel transmit system was designed as a retrofit for a 3 Tesla GE clinical research scanner, requiring a rapid and transparent switchover from a standard single channel transmitter. Two inputs were required from the host GE scanner: the input to the RF amplifier and the master exciter unblank (RF gate) signal. A single hard pulse played out from the scanner is divided eight ways and then modulated by an in-house built vector modulator [29]. The control system employs a PXI-7853R FPGA-based board with programs written in LabVIEW (National Instruments, Austin, TX) to drive the hardware and provide the baseband in-phase and quadrature signals to the vector modulator from the user-defined amplitude and phase information of each RF pulse [30]. The modulated waveforms pass through a first gain stage prior to the ultra-low output impedance amplifiers. The head array coil is connected to the amplifiers through transmit/receive switches. Low input impedance preamplifiers on the array coil provide the first gain stage on the receive side prior to passing through to the scanner receiver chain.

Array Fabrication

The eight-channel head array was designed with shielded rungs fabricated using copper sheet metal mounted to a ½ inch wide, 25 cm long acrylic piece with six breaks with 79 pF of capacitance at each break (Passive Plus, 1111C Series, Huntington, NY). The mounting piece for all the element hardware was a 12-inch outer diameter cylinder fabricated from white polycarbonate using a fusion deposition modeling (FDM) rapid prototyping machine.

The shield consisted of two layers of single-sided ½ ounce copper Pyralux (AC182500E, DuPont, Research Triangle Park, NC) mounted to the 12-inch cylinder. Each layer was slotted longitudinally to mitigate eddy currents and the two layers were oriented to alternate the position of the longitudinal slits. Rectangular slots were removed from the Pyralux shield and replaced with copper mesh to provide a view port through the coil for patient comfort and visual stimulus in functional imaging studies.

The elements were mounted on the inside of the cylinder with connections to the shield at one end and the matching network at the other. With the ½ inch thickness of the acrylic rung support and the ¼ inch thick cylinder, each rung was ¾ inch from the shield, creating an effective 10.5 inch diameter coil array. Shielded current probes were manufactured from 0.047 inch diameter semi-rigid (EZ 47-CU-SP, EZ Form Cable Corporation, Hamden, CT) to have an approximate loop diameter of ¼ inch. A small section of the outer conductor was removed to expose the inner conductor and enable B-field pick-up. The probes were placed adjacent to each rung, and the probe cable dropped down and connected to the RF shield along the length of the coil array. The probe signal was pulled out on the match and tune

board as shown in the diagram and photograph in Fig. 1. Baluns for both the element and current probe were mounted to the match and tune boards.

A single-sided ¼ ounce Pyralux end piece (AC091200EV) connected the shield segments near the top of the head to prevent RF fields from interacting with the rest of the transmit and receive chains. The transmit/receive switches and low-input impedance (R=1.5Ω) preamplifiers (WMA3RA, WanTCom Inc., Chanhassen, MN), were mounted to an acrylic piece covered in a ¼ ounce Pyralux ground plane. All hardware components were contained within a modular polycarbonate housing manufactured in-house using a 3D printer. A diagram of the array coil hardware with photos of the array and housing are shown in Fig. 2.

Coil Matching Network and Transmit/Receive Configuration

The matching network used to match and tune the coil elements to 50Ω is diagrammed in Fig. 3 [1]. Because the ULOI amplifier operates as the analog on the transmit side to the low-input impedance preamplifier on the receive side with respect to providing isolation, the matching network scheme is conveniently the same in both transmit and receive modes. The values for the matching network components were theoretically determined by the equations in [1] and then tuned to account for variations in practice. For each element, the capacitor C_x was selected to result in reasonable values for the remaining components that would not result in high voltages (small capacitance) or large currents (large capacitance) through the capacitors in the matching network. Adjustments in capacitors C_1 and C_2 were made to fine tune the coil. Tuning the trap was accomplished by short-circuiting the coil port (located on the match and tune board at the coil feed) to mimic the presence of the ULOI amplifier or preamplifier, placing the inductor L and the equivalent capacitance of the matching network in parallel to form a trap circuit. Slight adjustments to L were made to minimize S_{21} between a pair of two decoupled loop probes positioned near the rung, corresponding to minimum power being coupled into the coil – that is, when induced currents were suppressed and the amplifier or preamplifier was providing decoupling in the transmit and receive cases respectively. As seen in Fig. 3, the amplifier and preamplifier for each channel are connected to the rung by a PIN diode transmit/receive switch (UM9415, Microsemi, Aliso Viejo, CA) with typical insertion loss of -.2 dB and electrical length of .34λ in the transmit configuration. The total electrical length from the coil port to the preamplifier and amplifier accounted for a phase delay of a multiple of λ/2 to ensure the low impedance from the amplifier/preamplifier was presented to the coil port.

Measurements Overview

All measurements were conducted with a spherical phantom in place that mimicked the loading of an average human head. Because the decoupling benefits of ULOI amplifiers are realized by the impedance they present at the coil matching network port, it is not always appropriate to characterize or optimize with standard 50Ω port network analyzer measurements. If a measurement needs to be acquired which involves the amplifiers being connected in an “operational” configuration, then this requires the use of a more direct measurement of current on the rungs of the array rather than a port measurement. The measurements described below that rely on the impedance the amplifiers present were acquired with current probes in one of two configurations. Disambiguation will be ensured

by referring to them as “on-coil probes” or “crossed-probes”, representing respectively, the single current probe on each rung that is built into the coil (described above), or a pair of “free” crossed probes moveable to an individual rung. Three measurements are discussed in the sections that follow:

1. Characterizing the ULOI amplifiers: measuring the isolation per channel provided by the ULOI amplifiers, requiring a crossed-probe measurement on each channel
2. Characterizing the coil: measuring the on-coil decoupling added between elements, accomplished with a standard S_{21} port measurement under certain described conditions
3. Characterizing the system: measuring the total channel-to-channel coupling with the amplifiers connected, measured with the on-coil probes

Isolation from the Power Amplifiers

Because the amount of isolation provided by the power amplifier depends on its output impedance, the architecture is particularly sensitive to losses in the transmit cables and in-line transmit/receive switches. Ideally, the amplifiers might be placed at the coil and inside the bore [25], but to eliminate saturation and susceptibility effects from eight amplifiers with ferrite baluns, heat sinks, and MOSFET devices, as well as potential cooling problems, we opted to locate the power amplifiers outside the bore. This required a transmit cable to span the distance between the transmit/receive switch and the amplifier that maintained an electrical length of $n\lambda/2$ between the coil port and amplifier matching network. As expected, the losses associated with the added cable length and the transmit/receive switches reduce the achievable isolation from the amplifiers. Chu et al. discussed the effect of cable losses and observed that with a $7\lambda/2$ cable (insertion loss of 0.52 dB) at 3 Tesla, the isolation provided by the amplifier decreased to -9 dB as opposed to -14 dB obtained with the amplifier at the coil element [28]. For our particular setup, a $5\lambda/2$ transmit cable was required for each channel to place the amplifiers outside the bore.

Before measuring the isolation provided by the ULOI amplifier transmit system, the trap tuning on the coil was verified by measuring the ideal case with a short circuit at the coil port. An S_{21} measurement between a pair of crossed-probes positioned along the rung was used, with one probe exciting the rung, and the other sensing the field produced by the current on the rung. The isolation was calculated as the difference between S_{21} measurements collected with the coil port terminated in a 50Ω load and terminated in a short, in an analogous fashion to measuring the decoupling provided by an isolation preamplifier. With a short at the coil port, the isolation provided by the traps was observed to be -30 dB or better in all cases. The isolation provided by each amplifier was then measured using the same method. During the measurement the ULOI amplifier was connected to the coil and powered, with the input to the amplifier terminated in 50Ω. The isolation provided by each amplifier was calculated as the difference in the S_{21} measurements between a 50Ω load termination and termination with the amplifier connected through the transmit/receive switch and transmit cable. Based on these measurements, the average isolation provided by a well-tuned amplifier was found to be -11.5 dB with the $5\lambda/2$ transmit cable and transmit/receive switch in place. Using the same isolation measurement

method, the coil was instead terminated in the low-input impedance preamplifier with the transmit/receive switch in place. The isolation provided in this scenario (the receive case) was measured to be -20 dB or better for all elements.

To evaluate if the isolation provided by the amplifier independently provided sufficient decoupling between channels, the elements of the array coil were tuned individually with all other elements open-circuited as described above. The tuning of one element then was observed using an S_{11} measurement while the other elements were connected to the ULOI amplifiers. With the ULOI amplifiers, the element tuning shifted outside a standing-wave-ratio (SWR) of 2:1, indicating insufficient decoupling. While there are other possible solutions, we decided to add a simple capacitive decoupling network on the coil to augment the isolation provided by the amplifiers.

Providing Additional Decoupling Between the Elements

It is important to emphasize that the use of a conventional S_{21} port measurement to quantify coupling between elements is not always appropriate when using ULOI amplifiers, depending on the layout of any electrical connections between rungs. Specifically, the current distribution between two connected rungs is not always the same when a rung is terminated in the 50Ω network analyzer (as with a conventional port measurement) and when a rung is terminated in the high impedance provided by the trap circuit when the rung is connected to an ULOI amplifier (or preamplifier).

For clarification, Fig. 4 illustrates the effect of the different placement of the decoupling capacitor between elements of this particular array. Importantly, placing a decoupling capacitor between rungs at the feed end of the coil and performing a conventional S_{21} port measurement with a network analyzer could provide an inaccurate indication of the coupling between those rungs that would occur if they were fed by ULOI amplifiers. This can be understood more clearly by comparing the current paths in Fig. 4a and 4b, which illustrate the difference in resulting rung currents (and thus coupling) between termination in the 50Ω network analyzer and termination in an infinite impedance. As shown in Fig. 4c, placing the decoupling capacitor between rungs at the opposite end of the coil in front of the last distributed capacitor avoided this difference between the two termination cases and allowed for use of a direct S_{21} port measurement for setting the decoupling capacitor value between rungs. Placing a capacitor between the rungs changed the rung impedance slightly, requiring a second iteration to adjust matching network and trap tuning, as described above. It is important to emphasize the simplicity, however, of the single capacitor decoupling network that was enabled by the isolation provided by the ULOI amplifiers as compared to conventional on-coil decoupling networks.

Total Channel-to-Channel Isolation

To accurately measure total channel-to-channel isolation with the coil decoupling capacitors and amplifiers in place, the on-coil probes were used to measure the relative currents on the rungs. Two measurements were made in order to ensure valid probe measurements: one to determine the limit of meaningful detection and one to calibrate for the varying sensitivities between probes. To characterize the floor of meaningful measurements with the on-coil

probes, a setup with two neighboring rungs and probes was used. A network analyzer excited one rung, and the signal from both probes was measured with the adjacent rung open-circuited to limit induced current. This measurement detected the signal level sensed by both probes due to the field produced by the excited rung. The measurement indicated a "detection limit" of -24.5 dB between nearest neighbor probes. Therefore, nearest neighbor measurements made with the on-coil probes were capped at -24.5 dB.

In addition, the probes were calibrated to compensate for differences in probe sensitivity due to slight variations in loop size and orientation with respect to the rung. To do this, a test fixture was fabricated to position a second probe at a repeatable fixed height and orientation above each element. To collect a relative "sensitivity measurement" for each on-coil probe, all other elements were open-circuited, and the second probe was positioned above the respective element. A network analyzer was used to collect two S_{21} measurements: one between the element and the on-coil probe and one between the element and the second probe positioned above the element. The difference between the two measurements corresponded to the on-coil probe sensitivity and provided a set of calibration measurements for the eight probes. The measurements of the total channel-to-channel isolation obtained using the probes then were adjusted by this measurement.

To measure the isolation, one rung at a time was connected to the network analyzer and S_{21} measurements were collected between it and each of the eight on-coil probes. The measurements correlated to the relative currents on the rungs and thus to the element-to-element decoupling. In this manner 8x8 decoupling matrices (64 individual S_{21} measurements) were collected for two cases: 1) with the coil ports terminated in 50Ω, indicating the decoupling provided on the coil alone and 2) with the coil ports connected to the transmit system, indicating the total channel-to-channel isolation.

Imaging experiments were performed on a 3 Tesla GE Signa clinical research scanner. Each transmit channel was calibrated to 300 Watts at full scale input. Overall system performance was then demonstrated by acquiring B_1 maps from each channel operating at full scale. Mapping was done in the flood region of the American College of Radiology (ACR) phantom using the Bloch-Siegert method with a TR of 200 ms and a TE of 18 ms [31–33].

RESULTS AND DISCUSSION

The 8×8 decoupling matrices acquired with the rungs terminated in 50Ω and in the ULOI amplifiers are shown in Fig. 5. When the elements were terminated in 50Ω, the single capacitor decoupling network on the coil provided an average of -11 dB (-17.4 dB max, -6.9 dB min) of decoupling between nearest neighboring elements, as seen in Fig. 5a. The decoupling matrix acquired with the rungs terminated in the ULOI amplifiers is shown in Fig. 5b, indicating the added isolation provided by the amplifiers. The total average decoupling between channels with the amplifiers in line was -23.2 dB (-30.8 dB max, -13.9 min). Further iterative tuning of the amplifiers and/or of the decoupling between elements can certainly improve this, but sufficient independence between channels was considered to have been achieved based on observing a minimal shift in element tuning (within an SWR of

2:1) for all elements as compared to the original tuning that was done with all other elements open-circuited.

In a few cases, the coupling between next-nearest neighbors is higher than the coupling between nearest neighbors. This is due to the addition of a current path between these elements via the decoupling capacitor that was tuned for nearest-neighbor decoupling only. There are minor differences in the reciprocal measurements of the coupling matrices (i.e. $S_{ij} \neq S_{ji}$) due to the fact that all 64 measurements were acquired individually with the probes and therefore were sensitive to small differences in calibration.

The B_1 maps acquired from each element in the flood region of the ACR phantom are shown in Fig. 6. The patterns demonstrate an effective transmit system, generating well-isolated sensitivities and corroborating the expected behavior based on the coupling matrices.

CONCLUSION

In conclusion, we have discussed the design, construction, and characterization of the first eight-channel array coil for use with ultra-low output impedance amplifiers. In particular, considerations when adding decoupling to the array coil with respect to appropriate measurements and placement of the decoupling capacitor were detailed. The head array working with ultra-low output impedance amplifiers provided effectively isolated channels and avoided the need for complex on-coil decoupling, which is typically load dependent. The approach made a transmit/receive array configuration straightforward and demonstrates an option to consider for parallel transmission applications.

REFERENCES

1. Reykowski A, Wright SM, Porter JR. Design of matching networks for low noise preamplifiers. Magnetic Resonance in Medicine. 1995; 33(6):848–852. [PubMed: 7651124]
2. Edelstein W, et al. The intrinsic signal-to-noise ratio in NMR imaging. Magnetic Resonance in Medicine. 2005; 3(4):604–618. [PubMed: 3747821]
3. Ibrahim TS, et al. Effect of RF coil excitation on field inhomogeneity at ultra high fields: a field optimized TEM resonator. Magnetic resonance imaging. 2001; 19(10):1339–1347. [PubMed: 11804762]
4. Hoult DI. Sensitivity and Power Deposition in a High-Field Imaging Experiment. Journal of Magnetic Resonance Imaging. 2000; 12(1):46–67. [PubMed: 10931564]
5. Abraham R, Ibrahim TS. Proposed radiofrequency phased-array excitation scheme for homogenous and localized 7-Tesla whole-body imaging based on full-wave numerical simulations. Magnetic Resonance in Medicine. 2007; 57(2):235–242. [PubMed: 17260366]
6. Ibrahim TS, et al. Dielectric resonances and B ₁ field inhomogeneity in UHFMRI: computational analysis and experimental findings. Magnetic resonance imaging. 2001; 19(2):219–226. [PubMed: 11358660]
7. Kangarlu A, et al. Dielectric resonance phenomena in ultra high field MRI. Journal of computer assisted tomography. 1999; 23(6):821–831. [PubMed: 10589554]
8. Yang QX, et al. Analysis of wave Behavior in Lossy dielectric samples at high field. Magnetic Resonance in Medicine. 2002; 47(5):982–989. [PubMed: 11979578]
9. Collins CM, et al. Central brightening due to constructive interference with, without, and despite dielectric resonance. Journal of Magnetic Resonance Imaging. 2005; 21(2):192–196. [PubMed: 15666397]

10. Seifert, F.; Rinneberg, H. Adaptive coil control: SNR optimization of a TR volume coil for single voxel MRS at 3 T. Proceedings of the 10th Annual Meeting of ISMRM; Honolulu, Hawaii, USA. 2002.
11. Adriany G, et al. Transmit and receive transmission line arrays for 7 Tesla parallel imaging. Magnetic Resonance in Medicine. 2005; 53(2):434–445. [PubMed: 15678527]
12. Zhu Y, Giaquinto R. Improving flip angle uniformity with parallel excitation. Proc Int Soc Magn Reson Med. 2005
13. Ullmann P, et al. Experimental analysis of parallel excitation using dedicated coil setups and simultaneous RF transmission on multiple channels. Magnetic Resonance in Medicine. 2005; 54(4):994–1001. [PubMed: 16155886]
14. Katscher U, et al. Transmit SENSE. Magnetic Resonance in Medicine. 2003; 49(1):144–150. [PubMed: 12509830]
15. Zhu YD. Parallel excitation with an array of transmit coils. Magnetic Resonance in Medicine. 2004; 51(4):775–784. [PubMed: 15065251]
16. Grissom W, et al. Spatial domain method for the design of RF pulses in multicoil parallel excitation. Magnetic Resonance in Medicine. 2006; 56(3):620–629. [PubMed: 16894579]
17. Lee RF, Giaquinto RO, Hardy CJ. Coupling and decoupling theory and its application to the MRI phased array. Magnetic Resonance in Medicine. 2002; 48(1):203–213. [PubMed: 12111947]
18. Roemer P, et al. The NMR phased array. Magnetic Resonance in Medicine. 1990; 16(2):192–225. [PubMed: 2266841]
19. Jevtic, J. Ladder networks for capacitive decoupling in phased-array coils. Proceedings of the 9th Annual Meeting of ISMRM; Glasgow, Scotland. 2001.
20. Jevtic, J., et al. Design guidelines for the capacitive decoupling networks. Proc 11th Annual Meeting ISMRM; Toronto, ON, Canada. 2003.
21. Kurpad, K.; Boskamp, E.; Wright, S. Implementation of coil integrated RF power MOSFET as voltage controlled current source in a transmit phased array coil. Proceedings of the 12th Annual Meeting of ISMRM; Kyoto, Japan. 2004.
22. Kurpad, K.; Boskamp, E.; Wright, S. A parallel transmit volume coil with independent control of currents on the array elements. Proceedings 13th Scientific Meeting, International Society for Magnetic Resonance in Medicine; Miami Beach. 2005.
23. Kurpad KN, Wright SM, Boskamp EB. RF current element design for independent control of current amplitude and phase in transmit phased arrays. Concepts in Magnetic Resonance Part B-Magnetic Resonance Engineering. 2006; 29B(2):75–83.
24. Gudino, N., et al. 7T current-mode class-D (CMCD) RF power amplifier. Proceedings of the 17th Annual Meeting of ISMRM; Honolulu, HI. 2009.
25. Gudino N, et al. On-coil multiple channel transmit system based on class-D amplification and pre-amplification with current amplitude feedback. Magnetic Resonance in Medicine. 2012 p. n/a-n/a.
26. Kurpad, KN. Transmit field pattern control for high field magnetic resonance imaging with integrated RF current sources. Texas A&M University; 2012.
27. Heilman J, et al. Preamp-like decoupling and amplitude modulation in CMCD amplifiers for transmit arrays. Proc of Intl Soc Mag Reson Med. 2008; 1097
28. Chu X, et al. Ultra-Low Output Impedance RF Power Amplifier for Parallel Excitation. Magnetic Resonance in Medicine. 2009; 61(4):952–961. [PubMed: 19189287]
29. Hollingsworth, N., et al. An Easily Integrated Multichannel Modulator for All Field Strengths. 21st Annual Meeting of the International Society for Magnetic Resonance in Medicine; Salt Lake City, Utah. 2013.
30. Moody, KL., et al. Biomedical Imaging: From Nano to Macro, 2011 IEEE International Symposium on. IEEE; 2011. A LabVIEW-based operating system for parallel transmit systems.
31. Sacolick LI, et al. B1 mapping by Bloch-Siegert shift. Magnetic Resonance in Medicine. 2010; 63(5):1315–1322. [PubMed: 20432302]
32. Zhao F, et al. OPTIMIZED LINEAR COMBINATIONS OF CHANNELS FOR COMPLEX MULTIPLE-COIL B1 FIELD ESTIMATION WITH BLOCH-SIEGERT B1 MAPPING IN MRI.

33. Zhao, F., et al. Regularized estimation of magnitude and phase of multiple-coil B1 field via Bloch-Siegert B1 mapping. 20th Scientific Meeting of the International Society for Magnetic Resonance in Medicine; Melbourne, Australia. 2012.

HIGHLIGHTS

- Straightforward t/r configuration with decoupling amplifiers and preamplifiers
- Ultra-low output impedance amplifiers enable simplified on-coil decoupling
- Measurement considerations for isolation and coupling when using a non-50Ω system

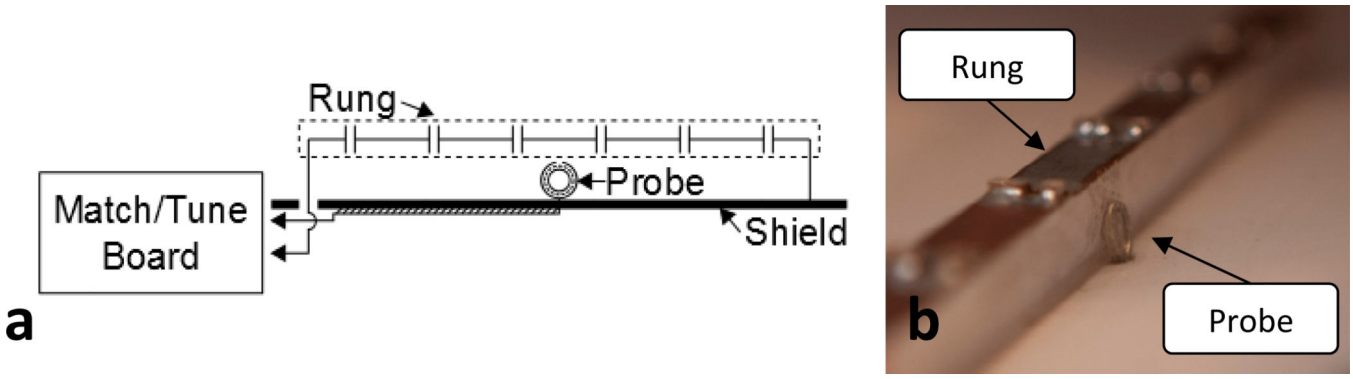

Figure 1.

(a) Diagram of the shielded probe and its location along the rung. The probe is at the center of the rung. The probe cabling is grounded to the RF shield and connects to the match and tune board at the far end of the coil. (b) Photograph of the shielded probe and location relative to the rung.

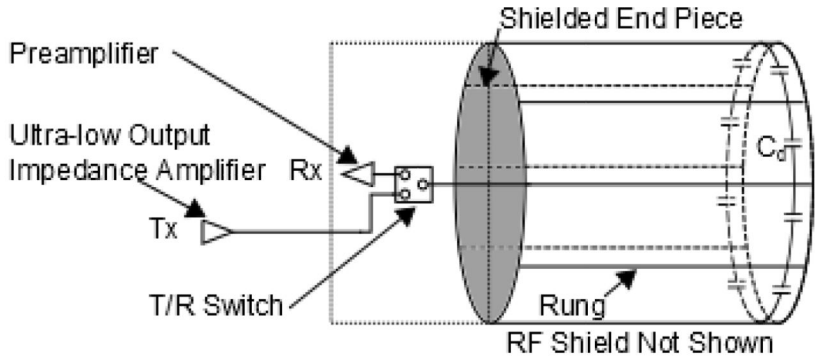

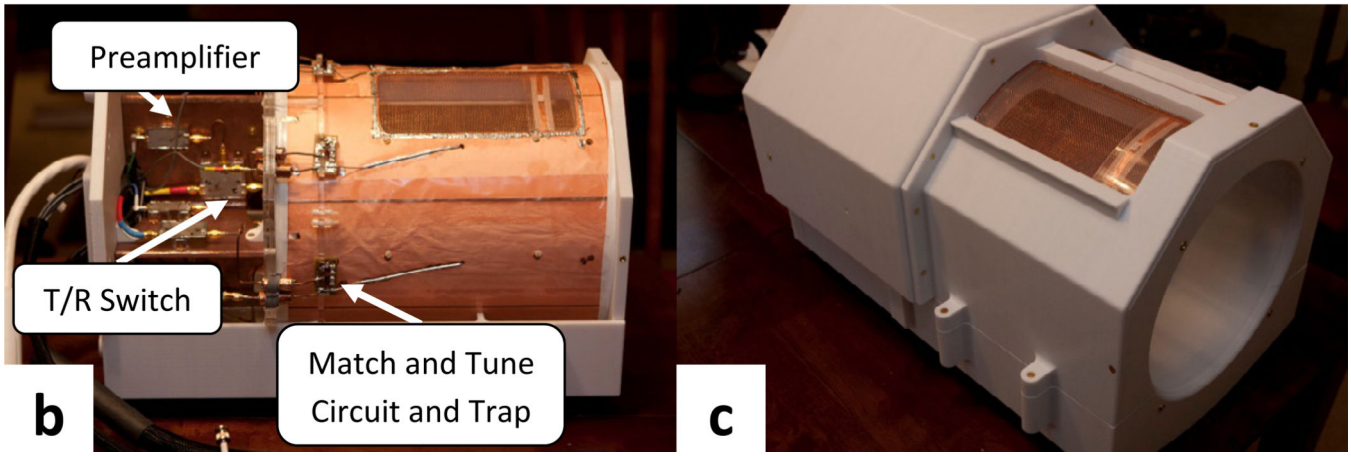

Figure 2.

(a) Diagram of the array coil setup showing the rung elements with the decoupling capacitor at the end opposite the coil feed. The preamplifiers and t/r switches are mounted on the coil as indicated and shown in b. The elements are shielded and a shielded end piece (labeled and shaded) prevents stray RF from interacting with the hardware behind. (b) Outside view of the array coil showing the array hardware. (c) Fully assembled array coil shown in its completed housing.

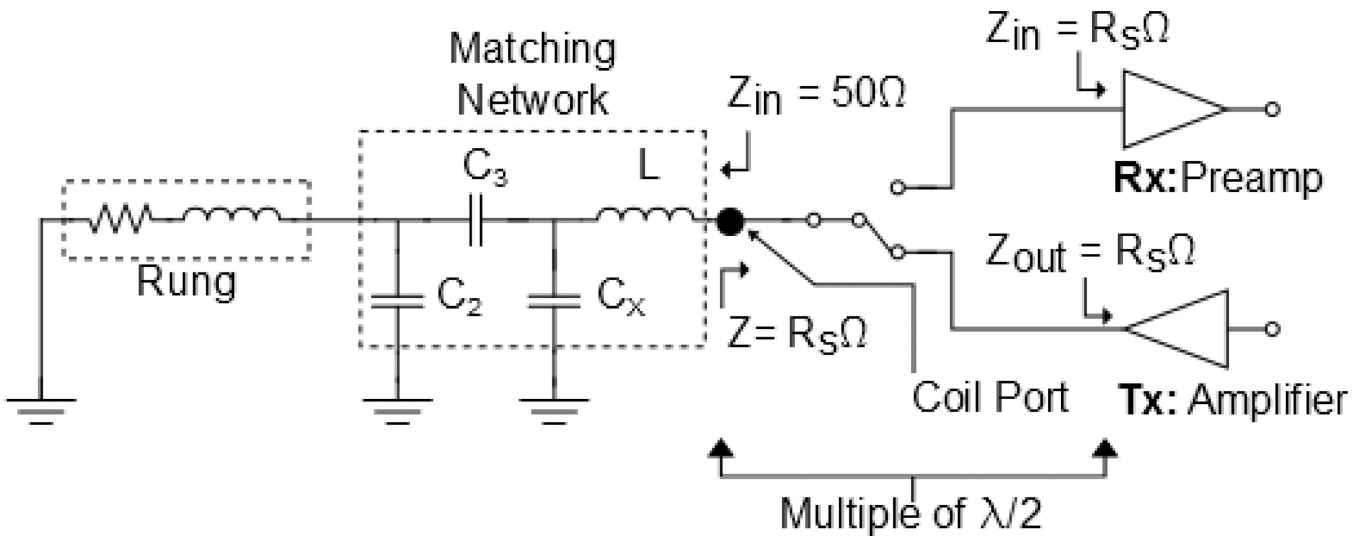

Figure 3.

Block diagram of the transmit/receive configuration of the array and matching network. During transmit and receive, the coil is presented with a low input impedance that places the inductor L in parallel with the equivalent capacitance of the matching network, creating a trap and suppressing induced currents. The electrical lengths between the coil port and the amplifier/preamplifier are a multiple of a half-wavelength to prevent an impedance transformation. The matching network used was presented in [1].

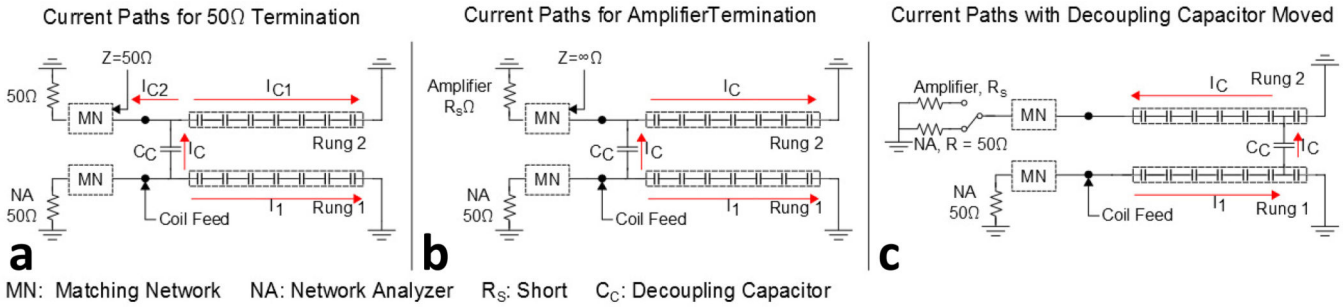

Figure 4.

Diagram showing the current paths for different decoupling capacitor placements to demonstrate appropriate coupling measurements when using ULOI amplifiers. (a) The decoupling capacitor is placed between the coil feeds and both coil ports are terminated in 50Ω (as is the case for a conventional S_{21} port measurement). The current path splits at the juncture between the rung and decoupling network and splits again at the connection to the adjacent rung due to the 50Ω termination. (b) Instead of a 50Ω load, the adjacent rung is terminated in the ULOI amplifier, labeled with theoretical infinite impedance. The current paths do not split at the adjacent rung, and the ratio of rung currents is different from the case shown in (a) indicating a difference in coupling. Therefore, if a conventional S_{21} measurement were used to choose the decoupling capacitor value, the coupling provided by the network would change in the operating case with the ULOI amplifier (or preamplifier). (c) The decoupling capacitor is placed in front of the last distributed capacitor to avoid the difference in current paths for the two terminations cases allowing for direct S_{21} port measurements to set the decoupling capacitor.

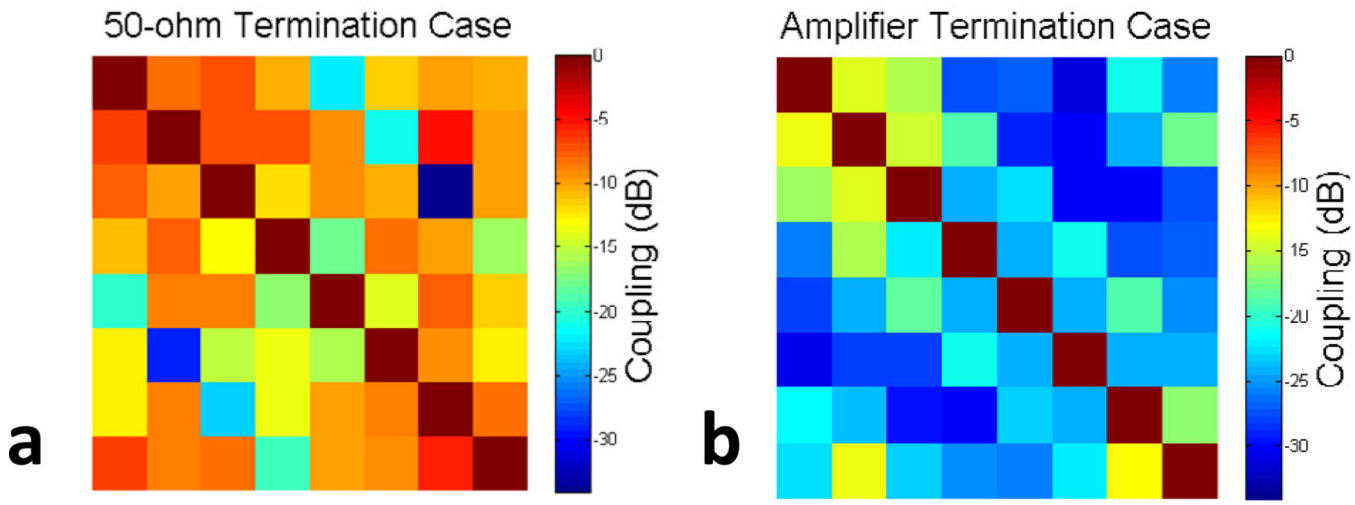

Figure 5.

Coupling matrices acquired using the on-coil current probes for the 50Ω and amplifier termination cases. (a) The coupling matrix acquired with the coil elements terminated in 50Ω loads. The decoupling network adds an average of -11 dB of decoupling between nearest neighbors to augment the isolation provided by the ULOI amplifiers. (b) The coupling matrix acquired with the coil terminated in the ultra-low output impedance amplifiers. With the amplifiers in line, overall channel-to-channel coupling is an average of -23.6 dB. Minor differences in the reciprocal measurements in both matrices (i.e $S_{ij} \neq S_{ji}$) are due to the fact that all 64 measurements were acquired individually and were therefore subject to slight differences in probe sensitivities.

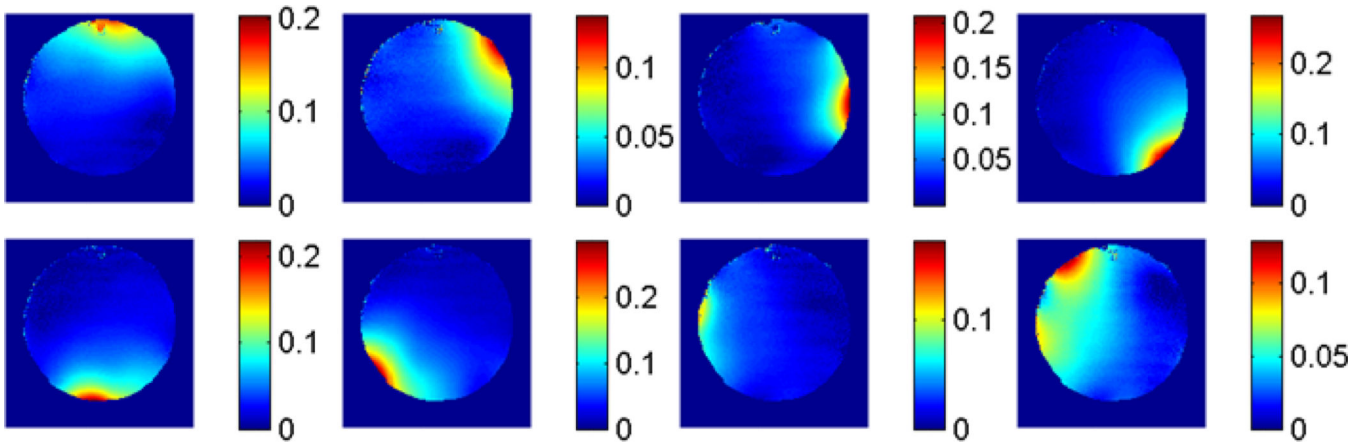

Figure 6.

B_1 maps in the flood region of the ACR phantom using the Bloch-Siegert method acquired using the eight channel array and ULOI amplifiers interfaced to a GE 3 Tesla clinical research scanner. The maps are scaled individually to better show the coil patterns and are shown in Gauss.